Journal of Alloys and Compounds 509 (2011) 4499–4504

Contents lists available at ScienceDirect

Journal of Alloys and Compounds

journal homepage: www.elsevier.com/locate/jallcom

Preparation of porous flower-like ZnO nanostructures and their gas-sensing property

Cuiping Gu[a], Jiarui Huang[a,b,*], Youjie Wu[a], Muheng Zhai[a], Yufeng Sun[c], Jinhuai Liu[b]

[a] College of Chemistry and Materials Science, Anhui Key Laboratory of Functional Molecular Solids, Anhui Normal University, Wuhu 241000, PR China
[b] Key Lab Biomimet Sensing & Adv Robot Technol, Institute of Intelligent Machines, Chinese Academy of Sciences, Hefei 230031, PR China
[c] Mechanical Engineering Department, Anhui University of Technology and Science, Wuhu 241000, PR China

ARTICLE INFO

Article history:
Received 17 July 2010
Received in revised form 6 November 2010
Accepted 11 November 2010
Available online 19 November 2010

Keywords:
Zinc oxide
Basic zinc carbonate
Flower-like
Porous
Gas sensor

ABSTRACT

Porous flower-like ZnO nanostructures have been synthesized by a template-free, economical hydrothermal method combined with subsequent calcination. Calcination of the precursors produced flower-like ZnO nanostructures, composed of interconnected porous ZnO nanosheets with high porosity resulting from the thermal decomposition of the as-prepared precursors, i.e., flower-like basic zinc carbonate (BZC). Moreover, the nanostructures have been characterized through X-ray diffraction, thermogravimetric-differential thermalgravimetric analysis, scanning electron microscopy, transmission electron microscopy, and Brunauer–Emmett–Teller N_2 adsorption–desorption analyses. Compared with ZnO nanorods, the as-prepared porous flower-like ZnO nanostructures exhibit a good response and reversibility to some organic gas, such as ethanol and acetone. The sensor responses to 100 ppm ethanol and acetone are 21.8 and 16.8, respectively, at a working temperature of 320 °C. In addition, the sensors also exhibited a good response to 2-propanol and methanol, which indicate that these porous flower-like ZnO nanostructures are highly promising for applications of gas sensors.

1. Introduction

Nanostructured ZnO materials have received considerable interest from scientists due to their remarkable performance in electronics, optics and photonics that are useful for dye sensitized solar cells [1], photocatalyst [2,3], gas sensors [4,5], etc. Up to now, various physical and chemical methods have been widely reported for the preparation of 1D (nanowires [6,7], nanorods [8,9], nanobelts [10], nanotubes [11], etc.) and complex (flower-like [12], rhombus-shaped [13], interconnected network-like [14], etc.) ZnO nanostructures. Some vapor methods, e.g., vapor transfer process [15] and thermal evaporation [16] are adopted to fabricate these materials. As one of the solution chemical routes, hydrothermal method [17] becomes a promising option for large-scale production, which is simpler, faster and less expensive.

In recent years, scientists have made some advancement in fabricating ZnO nanostructures using solution chemical routes. For example, Li et al. reported the growth of flower-like and cabbage-like nanostructures using CTAB as the surfactant in a hydrothermal growth process at different temperatures [18]. Manekkathodi et al. synthesized vertically aligned single-crystalline ZnO nanorods and nanoneedles on a paper substrate by the hydrothermal technique [19]. Yang et al. fabricated well-oriented ZnO nanorod arrays on different substrates via a hydrothermal method [20]. Gong et al. synthesized spindle-like ZnO microcrystals by a simple solution method at low temperature [21]. Sinha et al. reported on the preparation of a crystalline, pure hexagonal phase of ZnO as hollow spheroids in the presence of organic bases, such as pyridine, using zinc acetate as the precursor salt [22]. Park et al. reported on the preparation of ZnO nanoflowers by the solution-based hydrothermal growth method [23]. In our previous study, flower-shaped ZnO nanostructures were prepared by a simple solution route [24]. As mentioned above, various precursors and additives are used in aqueous medium to successfully synthesize ZnO nanostructures with different morphologies. These structures can be grown by tuning the growth rates along the fast growing directions [17]. The relative surface activities of various growth facets under given conditions determine the surface morphology of the grown structure.

Recently, two-dimensional porous ZnO nanostructures combining with unique sheet-like morphology and porous structure have been highly attracted by scientists because of their significantly enhanced properties in dye-sensitized solar cells and gas sensor applications. For example, Wang et al. reported on the synthesis of a porous hierarchical disk-like ZnO nanostructure fabricated via a simple low-temperature hydrothermal method for photovoltaic applications [25]. Qiu et al. reported on the facile hydrothermal

* Corresponding author at: College of Chemistry and Materials Science, Anhui Key Laboratory of Functional Molecular Solids, Anhui Normal University, 1# Beijing East Road, Wuhu 241000, PR China. Tel.: +86 553 3869 303; fax: +86 553 3869 303.
E-mail address: jrhuang@mail.anhu.edu.cn (J. Huang).

0925-8388/$ – see front matter © 2011 Published by Elsevier B.V.
doi:10.1016/j.jallcom.2010.11.078

preparation of hierarchically assembled, porous single-crystalline ZnO nanoplates and their application in dye-sensitized solar cells [26]. Jing and Zhan reported the gas sensor of hierarchically porous ZnO nanosheets mediated by microwave [27]. Zhang et al. reported the gas sensor of hierarchically three-dimensional (3D) porous ZnO architectures prepared by hydrothermal method combined with subsequent calcination [4]. In contrast with some other nanostructures, the hierarchically porous nanostructures can provide novel pattern for exploring unique properties and superior device performances. The conventional methods for preparing porous or hollow materials usually require the use of pore directing reagents or templates and may suffer from contamination due to the uncompleted removal of the additives either by chemical etching or thermal treatment [28,29]. Therefore, to develop facile, economical, template-free synthetic strategies to synthesize porous materials is of great significance from the view of both scientific research and practical application.

Here, porous flower-like ZnO nanostructures were synthesized by a template-free, economical hydrothermal method combined with subsequent calcination. The gas-sensing properties of the porous flower-like ZnO nanostructures were also discussed. The as-prepared pure ZnO microflowers with diameters and thickness of ca. 12–16 μm and 18 nm, respectively, can be observed. Furthermore, the porous flower-like ZnO nanostructures exhibit excellent gas-sensing sensor signals with test gases. A comparative gas sensing study between the as-prepared porous flower-like ZnO nanostructures and ZnO nanorods was performed to depict the superior sensing properties of the hierarchically porous ZnO material.

2. Experimental details

2.1. Synthesis

All chemical reagents used in this experiment were of analytical grade. The detailed synthesis procedures were described as follows. Zinc acetate hydrate ($Zn(OOCCH_3)_2{\cdot}2H_2O$, 0.01 mol) and $CO{-}(NH_2)_2$ (0.02 mol) were added to 30 ml of ethylene glycol (EG). The mixture solution was stirred, and the pH value of the resulting solution was adjusted to 5.0 using hydrochloric acid (HCl, 1 M) solution. Finally, the mixture solution was transferred into a 50 ml Teflon-lined autoclave. The autoclave was then filled with an appropriate amount of water up to 80% of the total volume and was kept inside an electric oven at 120 °C for 12 h. After naturally being cooled down, the white precipitate was centrifuged and washed with water and absolute ethanol several times, then dried at 80 °C for several hours. The final product of porous flower-like ZnO nanostructures was obtained by annealing the BZC precursor at 500 °C in a muffle furnace for 2 h.

For control experimental, ZnO nanorods were synthesized as follows. Zinc chloride ($ZnCl_2$, 0.613 g) was dissolved into 45 ml of deionized water. Then, the solution was stirred, and the pH value of the resulting solution was adjusted to 6.0 using ammonia (NH_4OH, 25 wt%) solution. The mixture was stirred for 30 min at about 180 r/min, and then the mixture solution was sealed in a Teflon-lined stainless-steel autoclave of 50 ml capacity. The autoclave was heated to and maintained at 180 °C for 10 h and then allowed to cool down to room temperature naturally. Finally, the white precipitate was centrifuged and washed with deionized water and absolute ethanol several times, then dried at 60 °C for 3 h.

2.2. Characterization

The products were characterized by X-ray diffraction (XRD, Shimadzu XRD-6000, with high-intensity Cu Kα radiation, wavelength 1.54178 Å), scanning electron microscopy (FE-SEM, Hitachi S-4800, operated at 5 kV), thermogravimetric analysis (TGA, SDT Q600, heating rate 10°/min in flow air), transmission electron microscopy (TEM, Hitachi H-800 with an accelerating voltage of 200 kV), and Brunauer–Emmett–Teller (BET) nitrogen adsorption–desorption (Nova 2000E). The pore-size distribution was determined from the adsorption branch of the isotherms using the Barett–Joyner–Halenda method.

2.3. Gas sensor fabrication and response test

The structures of the sensor device and the measurement system are similar to those of our previous report [29]. The as-prepared porous flower-like ZnO nanostructures and ZnO nanorods dispersed in ethanol solution were directly coated on the outer surface of an alumina tube-like substrate by a pipette on which a pair of Au electrodes had been printed previously, followed by drying at 60 °C for about 2 h and subsequent annealing at 360 °C for about 2 h. Finally, a small Ni–Cr alloy coil was inserted into the tube as a heater, which provided the working temperature of the gas sensor.

In order to improve the long-term stability, the sensors were kept at the working temperature (320 °C) for 2 days. A stationary state gas distribution method was used for testing gas response in dry air. The test was operated in a measuring system of ART-2000A (Art Beijing Science and Technology Development Co., Ltd., PR China). Detecting gases, such as ethanol vapor, were injected into a test chamber and mixed with air. The gas response of the sensor in this paper was defined as $S = R_a/R_g$ (reducing gases), where, R_a is the resistance in dry air and R_g is that in the dry air mixed with detected gases. In our measurement system, the gas response of the sensor also can be calculated by the following equation: $S = (V_{gas}(5000\ \text{mV} - V_{air}))/(V_{air} \cdot (5000\ \text{mV} - V_{gas}))$, where V_{air} and V_{gas} were the output voltages in air and test gas, respectively. The response or recovery time was expressed as the time taken for the sensor output to reach 90% of its saturation after applying or switching off the gas in a step function.

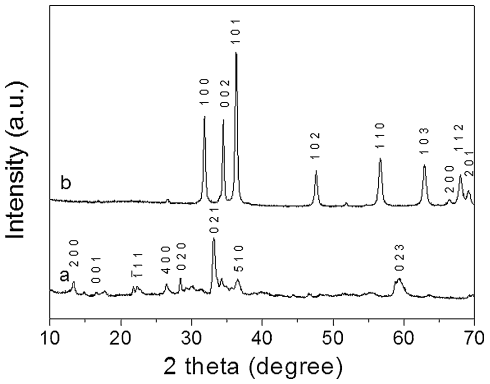

Fig. 1. XRD patterns of (a) BZC precursor and (b) calcined ZnO product of the BZC precursor.

3. Results and discussion

3.1. Structure and morphology

The porous flower-like ZnO nanostructures were obtained through a two-step procedure. First, a basic zinc carbonate (BZC) precursor with a microflower structure was obtained from a hydrothermal process. Then calcination of the precursor yielded flower-like ZnO nanostructures that were assembled by porous ZnO nanosheets. The crystal phase of the BZC precursor was characterized by XRD, and the data are shown in Fig. 1a. All the diffraction peaks of the precursors can be indexed as monoclinic hydrozincite $Zn_5(CO_3)_2(OH)_6$ (JCPDS 19-1458), which is in good accordance with the recent report [4]. Fig. 1b shows the XRD pattern of the calcined ZnO product (500 °C, 2 h), with a perfect indexation as hexagonal wurtzite ZnO (JCPDS 36-1451).

TG-DTA investigations were conducted to determine the thermal behavior of the obtained BZC microflowers, and the data are shown in Fig. 2. The DTA plot presents one endothermic peak at 236 °C which corresponds to the weight loss stage (Fig. 2). The total weight loss of 26.5% attributed to the decomposition of carbonate and hydroxide in the precursor matches well with the expected theoretical value (25.9%).

Fig. 3 displays the FTIR spectra of the BZC precursor and ZnO product, showing that the spectra are significantly different from each other. Especially, those peaks at 708, 834, 1397, 1500 cm^{-1} (Fig. 4a) corresponding to the bending vibration of CO_3^{2-} have disappeared or severely weakened in Fig. 4b, indicating the decomposition of carbonate in the precursor. In addition, the peak at 3330 cm^{-1} (Fig. 3a) related to the large amount of –OH in the precursor is substituted by a much weaker peak at 3458 cm^{-1} (Fig. 3b) attributed to surface absorbed water after calcination.

The morphology of the precursor before and after calcination is characterized by SEM. Fig. 4 displays the SEM images of the BZC pre-

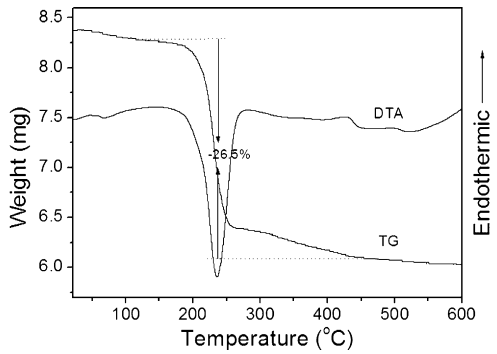

Fig. 2. TG-DTA analysis of the BZC precursor.

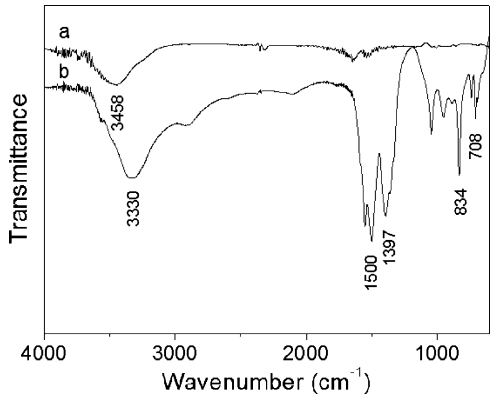

Fig. 3. FTIR data of (a) BZC precursor and (b) corresponding calcined ZnO product.

cursor and the corresponding ZnO product after calcination. As can be seen at lower magnification (Fig. 4a), the precursor consists of relatively uniform flower-like nanostructures with an average size of 14 μm. In addition, these nanostructures are sufficiently stable so that they could not be broken into discrete nanosheets, even after ultrasonication for a long time. At higher magnification (Fig. 4b), tens of layers of assembled thin nanosheets in the 3D nanostructures could be clearly observed. Careful examination reveals that these BZC nanosheets are 3–8 μm in length and width and about 20 nm in thickness. Fig. 4c and d displays the SEM images of the as-prepared flower-like ZnO nanostructures after thermal treatment of the precursor at 500 °C for 2 h. It is found that most of the productions well maintain the flower shape of the precursor without significant collapse after calcination. Unlike the work reported by Zhang et al. [4], the pore structures in our ZnO nanosheets are visible from SEM images (Fig. 4d). This is probably due to the much thinner thickness (20 nm) of our BZC nanosheets compared with their tens to hundreds of nanometers thickness. Furthermore, detailed observation from the TEM images (Fig. 5) clearly confirms the high porosity of the ZnO nanosheets, which resulted from the thermal decomposition of carbonate and hydroxide of the precursor. As can be seen, a large amount of irregular pores of tens of nanometers are randomly distributed in the nanosheets.

To further confirm the inner architectures of the porous flower-like ZnO nanostructures, nitrogen adsorption and desorption measurements were performed to estimate the texture properties. The nitrogen adsorption and desorption isotherm and pore size distribution curve (inset) of hierarchically porous ZnO nanostructures calcined at 500 °C are shown in Fig. 6. The isotherm of the hierarchically porous ZnO nanostructure sample exhibits a hysteresis loop at the p/p_0 ranges of 0.34–0.96, which is associated with the filling and emptying of mesopore by capillary condensation. The characteristic feature of these curves is their hysteresis loop, which does not exhibit any limiting adsorption at high relative pressures. According to the IUPAC classification, the loop observed is ascribed to type H3 loops, indicating the presence of mesopores (pores 3–48 nm in

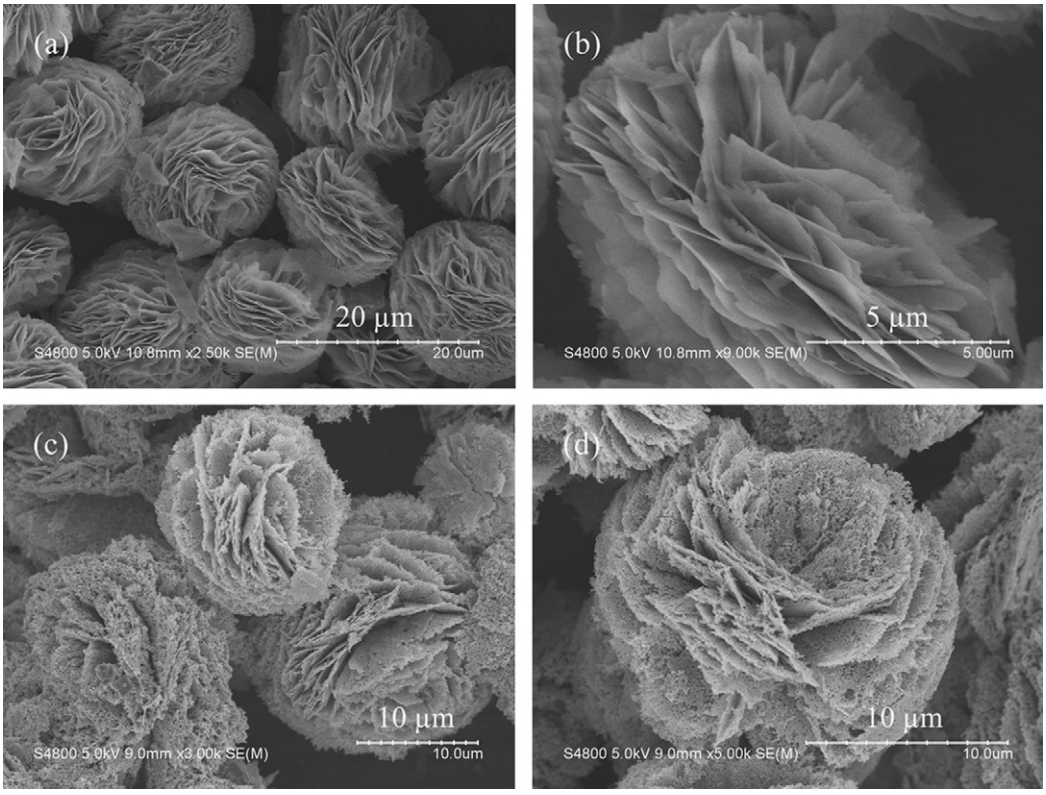

Fig. 4. Representative SEM images of (a and b) flower-like BZC precursor and (c and d) corresponding calcined porous flower-like ZnO nanostructures.

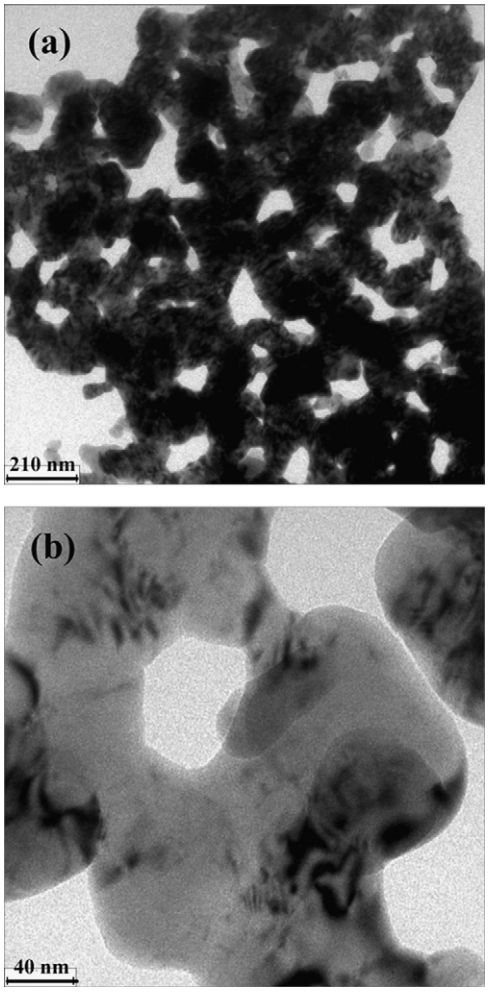

Fig. 5. TEM images of the porous ZnO nanosheet calcined BZC precursor (a and b).

diameter) in the material. Using the BJH method and the desorption branch of the nitrogen isotherm, the calculated pore-size distribution indicates that the material contains an average pore size of 16.5 nm. Pores of various sizes were observed in the TEM image, in accordance with these stochastic calculation results. The BET surface area of the hierarchically porous ZnO nanostructures can be calculated to be 8.6 $m^2\ g^{-1}$, which is much bigger than the surface area of ZnO nanorods (3.3 $m^2\ g^{-1}$).

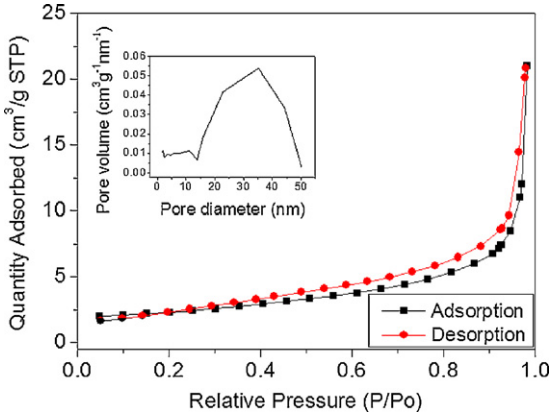

Fig. 6. N_2 adsorption–desorption isotherm and BJH pore size distribution plots (inset) of the porous ZnO product calcined BZC precursor.

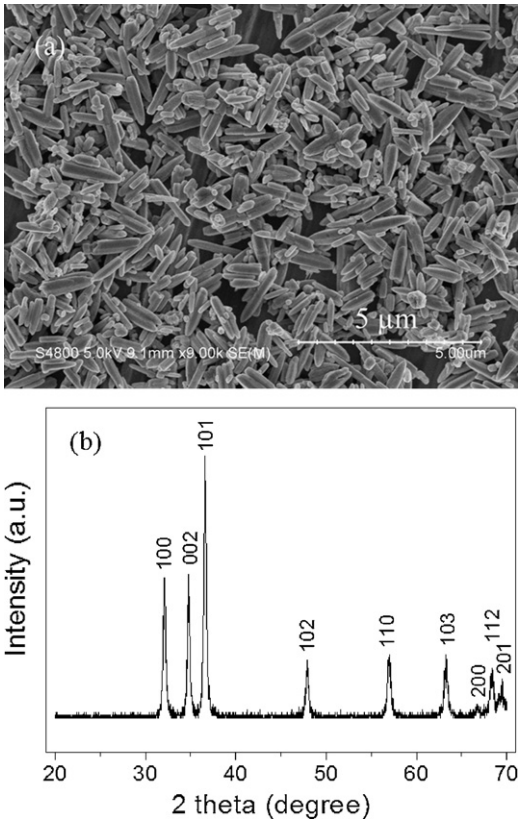

Fig. 7. (a) SEM images of the ZnO product from control experiment and (b) XRD pattern of the ZnO product from control experiment.

For control experimental, ZnO nanorods were synthesized by hydrothermal method. The SEM images of the product are exhibited in Fig. 7a, showing that only ZnO nanorods were produced. The diameter of ZnO nanorods normally ranges from 300 to 600 nm and the lengths are 1–2 μm. The XRD pattern is shown in Fig. 7b implying that the obtained product is hexagonal wurtzite ZnO (JCPDS 36-1451).

3.2. Gas-sensing properties of the porous flower-like ZnO nanostructures

Hierarchical or porous semiconductor metal oxides are promising materials for gas sensor. Their special structures can usually provide a large surface-to-volume ratio, which is most favorable for the diffusion of target gases in sensor materials. Many studies have proven that these special structures could significantly enhance the sensor performance. In addition, the high porosity of the as-prepared hierarchically porous architectures provides excellent channels and "surface accessibility" for the mass transportation of target gases. Because of these advantages that are not available from bulk or solid materials, the as-prepared flower-like porous nanostructures are expected to exhibit excellent properties for gas sensor applications.

The gas sensors are fabricated from the as-prepared porous flower-like ZnO nanostructures and ZnO nanorods for comparison. Panels a and b of Fig. 8 show the real-time response curves and the sensor responses of the sensor devices upon exposure to different concentrations of ethanol at a working temperature of 320 °C, respectively. The as-prepared porous flower-like ZnO nanostructures have a good response to ethanol. At a low concentration of 5 ppm of ethanol, the relative response is approximately 4.8. When increasing the concentration, the response of the sensor also

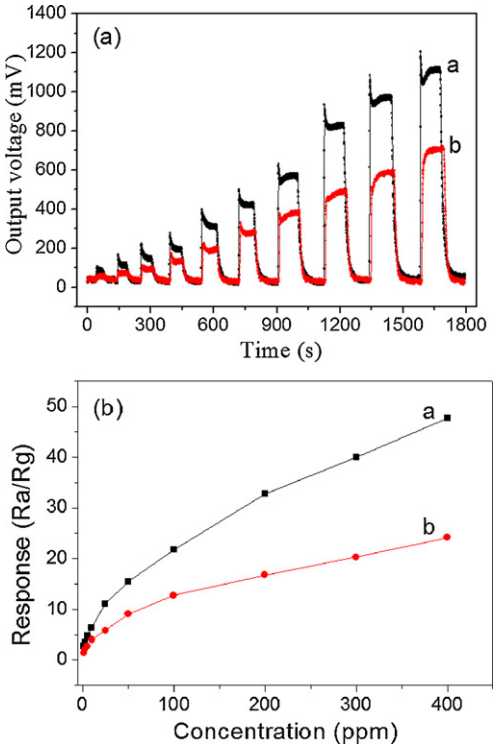

Fig. 8. Real-time response curves (a) and sensor responses (b) of the sensors based on the porous flower-like ZnO nanostructures (lines a) and ZnO nanorods (lines b) upon exposure to different concentrations of ethanol at a working temperature of 320 °C.

sharply increased, as shown in Fig. 4b. The response to 100 ppm ethanol is up to 21.8, and the response time and recovery time were about 3 s and 12 s, respectively. Furthermore, according to Fig. 8a, it can be observed that the sensor also has a good reversibility. In the same measurement system, the ZnO nanorods also have good responses to ethanol as shown in Fig. 8a. But the responses of ZnO nanorods to ethanol are much lower than those of the porous flower-shaped ZnO nanostructures. In addition, the response of the porous flower-like ZnO nanostructures is also much higher than those of ZnO nanowires [30], nanorods [31], porous nanoplates [27], and flowerlike ZnO structures composed of rods [32]. Furthermore, the sensors fabricated with porous flower-shaped ZnO nanostructures and ZnO nanorods also show a significant response to acetone, 2-propanol and methanol, as shown in Supplementary data, Figs. S1 and S2, respectively. The responses of porous flower-shaped ZnO nanostructures to 100 ppm of acetone, 2-propanol and methanol are about 16.8, 17.2 and 10.4, respectively. The responses of ZnO nanorods to 100 ppm acetone, 2-propanol and methanol are 5.6, 8.5 and 5.8, respectively, which are much lower than those of the porous flower-shaped ZnO nanostructures as shown in Fig. 9. These results demonstrate that the porous flower-shaped ZnO nanostructures show higher sensitivity to detect organic vapors at low concentrations compared with the nanorods. However, the particular structures have not obviously improved the sensitivity of the ZnO gas sensors. Selectivity is very important in the gas sensing application. Further study should be focused on improving the sensitivity of the ZnO nanostructure gas sensors by doping of noble metals (Pt, Pd, Au, etc.). In addition, temperature modulation is also a selective method for improving the selectivity of the metal oxide gas sensors [33].

From Fig. 8a, it is obvious that the gas sensor exhibits rapid gas-sensing behaviors when the target gases are injected or released. This can be explained from the aspect of gas diffusion [29]. The gas diffusion is directly proportional to the porosity and pore diameter,

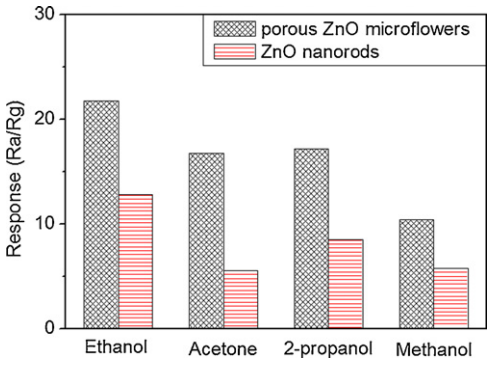

Fig. 9. Responses of the sensors based on two kinds of ZnO nanostructures upon exposure to four kinds of organic vapors (100 ppm) at a working temperature of 320 °C.

while it is inversely proportional to the pore tortuosity. BET analysis has revealed an average pore diameter of the hierarchically porous ZnO nanostructures of about 16.5 nm. Besides, the tortuous pore network has been investigated by observations of the morphology of porous flower-like ZnO nanostructures. The current flow would go through the contacts between the outer ends of the porous nanosheets, as shown in Supplementary data, Fig. S3. Hence, the porous flower-like ZnO nanostructure film is suggested to allow fast diffusion of gas molecules, resulting in the high rates of gas adsorption and desorption. This could be considered as a contributor to the highly sensitive performance of the as-fabricated gas sensor. So, the porous flower-like ZnO nanostructures are observed to demonstrate better sensitivity to the organic vapors. Meanwhile, an additional two sensors were fabricated under the same process. Similar gas-sensing properties were obtained, which suggest the good repeatability of the sensors.

4. Conclusions

A template-free hydrothermal method combined with a subsequent annealing process was demonstrated for the synthesis of porous flower-like ZnO nanostructures. Gas sensors were fabricated from the as-synthesized porous flower-like ZnO nanostructures and applied to detecting some organic vapors. Comparative gas sensing tests between gas sensors based on porous flower-like ZnO nanostructures and ZnO nanorods clearly show that the former exhibits more excellent sensing performances, implying a good potential of the porous flower-like ZnO nanostructures for sensor applications. The enhanced sensing performances are attributed to the high porosity and 3D morphology, which can significantly facilitate gas diffusion and mass transportation in sensing materials.

Acknowledgements

This work has been supported by National Basic Research Program of China (973 Program 2007CB936602, 2011CB933700), Young College Teachers' Research Fund Program of Anhui Normal University (Project NO. 2009xqn70, 2009xqn71), and Anhui provincial natural science (Project NO. 090412036).

Appendix A. Supplementary data

Supplementary data associated with this article can be found, in the online version, at doi:10.1016/j.jallcom.2010.11.078.

References

[1] A. Qurashi, M.F. Hossain, M. Faiz, N. Tabet, M.W. Alam, N.K. Reddy, J. Alloys Compd. 503 (2010) L40.
[2] M.S. Mohajerani, A. Lak, A. Simchi, J. Alloys Compd. 485 (2009) 616.
[3] N. Kaneva, I. Stambolova, V. Blaskov, Y. Dimitriev, S. Vassilev, C. Dushkin, J. Alloys Compd. 500 (2010) 252.
[4] J. Zhang, S.R. Wang, M.J. Xu, Y. Wang, B.L. Zhu, S.M. Zhang, W.P. Huang, S.H. Wu, Cryst. Growth Des. 9 (2009) 3532.
[5] C.D. Lokhande, P.M. Gondkar, R.S. Mane, V.R. Shinde, S.H. Han, J. Alloys Compd. 1475 (2009) 304.
[6] Y.X. Du, Q.X. Yuan, J. Alloys Compd. 494 (2010) 468.
[7] Y. Liu, Z.H. Kang, Z.H. Chen, I. Shafiq, J.A. Zapien, I. Bello, W.J. Zhang, S.T. Lee, Cryst. Growth Des. 9 (2009) 3222.
[8] X.F. Ma, A.Y. Liu, H.Z. Xu, G. Li, M. Hu, G. Wu, Mater. Res. Bull. 43 (2008) 2272.
[9] S.K. Park, J.H. Park, K.Y. Ko, S. Yoon, K.S. Chu, W. Kim, Y.R. Do, Cryst. Growth Des. 9 (2009) 3615.
[10] Y.G. Wei, Y. Ding, C. Li, S. Xu, J.H. Ryo, R. Dupuis, A.K. Sood, D.L. Polla, Z.L. Wang, J. Phys. Chem. C 112 (2008) 18935.
[11] B. Liu, H.C. Zeng, Nano Res. 2 (2009) 201.
[12] Q.A. Li, H.K. Sun, M. Luo, W.J. Weng, K. Cheng, C.L. Song, P.Y. Du, G. Shen, G.R. Han, J. Alloys Compd. 503 (2010) 514.
[13] F. Xu, Y.N. Lu, L.T. Sun, L.J. Zhi, Chem. Commun. 46 (2010) 3191.
[14] N.S. Yu, D.M. Deng, D. Yang, Y. Wang, T.P. Yang, J. Alloys Compd. 505 (2010) L27.
[15] Z.M. Zhu, T.L. Chen, Y. Gu, J. Warren, R.M. Osgood, Chem. Mater. 17 (2005) 4227.
[16] A. Umar, S.H. Kim, J.H. Kim, A. Al-Hajry, Y.B. Hahn, J. Alloys Compd. 463 (2008) 516.
[17] S. Baruah, J. Dutta, Sci. Technol. Adv. Mater. 10 (2009) 013001.
[18] F. Li, L. Hu, Z. Li, X.T. Huang, J. Alloys Compd. 465 (2008) L14.
[19] A. Manekkathodi, M.Y. Lu, C.W. Wang, L.J. Chen, Adv. Mater. 22 (2010) 4059.
[20] J.H. Yang, J.H. Zheng, H.J. Zhai, X.M. Yang, L.L. Yang, Y. Liu, J.H. Lang, M. Gao, J. Alloys Compd. 489 (2010) 51.
[21] L.H. Gong, X. Wu, C. Ye, F.Y. Qu, M.Z. An, J. Alloys Compd. 501 (2010) 375.
[22] A.K. Sinha, M. Basu, M. Pradhan, S. Sarkar, T. Pal, Chem. Eur. J. 16 (2010) 7865.
[23] J.K. Park, Y.J. Kim, J. Yeom, J.H. Jeon, G.C. Yi, J.H. Je, S.K. Hahn, Adv. Mater. 22 (2010) 4059.
[24] J.R. Huang, Y.J. Wu, C.P. Gu, M.H. Zhai, K. Yu, M. Yang, J.H. Liu, Sens. Actuators B 146 (2010) 206.
[25] J.X. Wang, C.M.L. Wu, W.S. Cheung, L.B. Luo, Z.B. He, G.D. Yuan, W.J. Zhang, C.S. Lee, S.T. Lee, J. Phys. Chem. C 114 (2010) 13157.
[26] Y.C. Qiu, W. Chen, S.H. Yang, J. Mater. Chem. 20 (2010) 1001.
[27] Z.H. Jing, J.H. Zhan, Adv. Mater. 20 (2008) 4547.
[28] X.W. Lou, L.A. Archer, Z.C. Yang, Adv. Mater. 20 (2008) 3987.
[29] J.R. Huang, K. Yu, C.P. Gu, M.H. Zhai, Y.J. Wu, M. Yang, J.H. Liu, Sens. Actuators B 147 (2010) 467.
[30] W.Y. Wu, J.M. Ting, P.J. Huang, Nanoscale Res. Lett. 4 (2009) 513.
[31] Z.P. Sun, L. Liu, L. Zhang, D.Z. Jia, Nanotechnology 17 (2006) 2266.
[32] P. Feng, Q. Wan, T.H. Wang, Appl. Phys. Lett. 87 (2005) 213111.
[33] J.R. Huang, G.Y. Li, Z.Y. Huang, X.J. Huang, J.H. Liu, Sens. Actuators B 114 (2006) 1059.